Antiviral Research 168 (2019) 175–182

Contents lists available at ScienceDirect

Antiviral Research

journal homepage: www.elsevier.com/locate/antiviral

Heterologous expression of human norovirus GII.4 VP1 leads to assembly of T = 4 virus-like particles

Jessica M. Devant[a,b], Götz Hofhaus[c], David Bhella[d], Grant S. Hansman[a,b,*]

[a] Schaller Research Group at the University of Heidelberg and the DKFZ, Heidelberg, Germany
[b] Department of Infectious Diseases, Virology, University of Heidelberg, Heidelberg, Germany
[c] Bioquant, CellNetWorks, University of Heidelberg, Heidelberg, Germany
[d] MRC, University of Glasgow Centre for Virus Research, Glasgow, Scotland, UK

ABSTRACT

Human noroviruses are a leading cause of acute gastroenteritis, yet there are still no vaccines or antivirals available. Expression of the norovirus capsid protein (VP1) in insect cells typically results in the formation of virus-like particles (VLPs) that are morphologically and antigenically comparable to native virions. Indeed, several different norovirus VLP candidates are currently used in clinical trials. So far, structural analysis of norovirus VLPs showed that the capsid has a T = 3 icosahedral symmetry and is composed of 180 copies of VP1 that are folded into three quasi-equivalent subunits (A, B, and C). In this study, the VLP structures of two norovirus GII.4 genetic variants that were identified in 1974 and 2012 were determined using cryo-EM. Surprisingly, we found that greater than 95% of these GII.4 VLPs were larger than virions and 3D reconstruction showed that these VLPs exhibited T = 4 icosahedral symmetry. We also discovered that the T = 4 VLPs presented several novel structural features. The T = 4 particles assembled from 240 copies of VP1 that adopted four quasi-equivalent conformations (A, B, C, and D) and formed two distinct dimers, A/B and C/D. The protruding domains were elevated ~21 Å off the capsid shell, which was ~7 Å more than in the previously studied GII.10 T = 3 VLPs. A small cavity and flap-like structure at the icosahedral two-fold axis disrupted the contiguous T = 4 shell. Overall, our findings indicated that GII.4 VP1 sequences assemble into T = 4 VLPs and these larger particles might have important consequences for VLP-based vaccine development.

1. Introduction

Human noroviruses are members of the *Caliciviridae* family and are a leading cause of outbreaks of acute gastroenteritis. The virus has a positive sense, single stranded RNA genome of ~7.7 kbp. The genome is organized in three open reading frames (ORFs), where ORF1 encodes nonstructural proteins and ORF2 and ORF3 encode a major structural protein (termed VP1) and a minor structural protein (termed VP2), respectively. Noroviruses are genetically diverse and based on VP1 sequences have been classified into seven genogroups (GI-GVII), where GI, GII, and GIV cause infections in humans (Vinje, 2015; Hansman et al., 2006). The GI and GII are further subdivided into numerous genotypes, with GII genotype 4 (GII.4) recognized as the most prevalent and clinically important strain (Donaldson et al., 2008; Ramani et al., 2014).

Recently, two human norovirus cell culture systems were developed (Ettayebi et al., 2016; Jones et al., 2014). However, mechanistic studies of norovirus structure and biology, such as interaction with the host receptor(s), remain challenging owing to difficulties in large-scale virion preparations. Nevertheless, expression of ORF2 in insect or mammalian cells can result in the formation of virus-like particles (VLPs) that are antigenically and morphologically similar to native virions (Hansman et al., 2006, 2012; Prasad et al., 1994, 1999; Lawton et al., 1997). These VLPs have permitted studies on host binding factors, interactions with norovirus-specific antibodies and structural studies (Hansman et al., 2006; Lindesmith et al., 2011, 2012, 2013; Ajami et al., 2012; Bok et al., 2009; Baric et al., 2002). Indeed, histo-blood group antigens (HBGAs) and bile acids were shown to be important binding co-factors for human norovirus VLPs and/or virions (Ettayebi et al., 2016; Hutson et al., 2002; Marionneau et al., 2002; Tan and Jiang, 2005; Tan et al., 2003; Kilic et al., 2019). Moreover, norovirus VLPs are currently used as vaccine candidates. Clinical studies using different genogroups, including a consensus VP1 sequence of GII.4 (termed GII.4c) have shown some promising results, even though protection is limited (Parra et al., 2012; Bernstein et al., 2015).

Structural analysis of GI.1 VLPs revealed that VP1 is separated into two distinct domains: a shell domain (S domain) that encloses the RNA and a protruding domain (P domain) that binds to co-factors, such as HGBAs and bile acids (Prasad et al., 1999; Tan and Jiang, 2005; Kilic et al., 2019). A hinge region, which is typically composed of 10–14 amino acids, connects the S and P domains. The P domain has a β-barrel fold that is structurally conserved in the *Caliciviridae* family. Dimerization of the P domains forms arch shaped protrusions that are visible in electron microscopy images. The P domain is further subdivided into

* Corresponding author. CHS Foundation, University of Heidelberg, and German Cancer Research Center, Heidelberg, Germany.
E-mail address: g.hansman@dkfz.de (G.S. Hansman).

https://doi.org/10.1016/j.antiviral.2019.05.010
Received 10 April 2019; Received in revised form 21 May 2019; Accepted 24 May 2019
Available online 27 May 2019
0166-3542/

P1 and P2 subdomains, where the P2 subdomain is an insertion in the P1 subdomain and is the most variable region on the capsid (Prasad et al., 1999).

Structural studies have shown that caliciviruses have a common overall organization of T = 3 icosahedral symmetry and are comprised of 180 copies of VP1 (Hansman et al., 2012; Prasad et al., 1999; Bhella and Goodfellow, 2011; Chen et al., 2004; Conley et al., 2017). Within the asymmetric unit, VP1 adopts three quasi-equivalent conformations, termed A, B, and C (Prasad et al., 1999). The norovirus A and B subunits assemble into 60 dimers (termed A/B) at the quasi two-fold axis, whereas the C subunits assemble into 30 C/C dimers that are located at the strict icosahedral two-fold axis. In the GI.1 VLPs, the A/B dimers have a convex S domain conformation, whereas the C/C dimers have a flat S domain conformation (Prasad et al., 1999). The conformational differences within these dimers likely facilitate the curvature of the virus particle to form a closed shell; such features are commonly seen in other T = 3 icosahedral viruses (Prasad and Schmid, 2012). Interestingly, smaller norovirus VLPs (~25 nm in diameter) that are assumed to have a T = 1 icosahedral symmetry have also been reported (Ettayebi et al., 2016; Taniguchi et al., 1981).

Here, we solved the cryo-EM structures of VLPs for two GII.4 variants that were identified in 1974 and 2012, termed CHDC-1974 and NSW-2012, respectively (Bok et al., 2009; Eden et al., 2013). We show that these VLPs have a T = 4 icosahedral symmetry and are composed of 240 copies of VP1. In order to form the T = 4 icosahedral structure, VP1 adopts four quasi-equivalent conformations, termed A, B, C, and D, giving rise to two distinct types of dimers, termed A/B and C/D. The VLPs consisted of 60 A/B dimers and 60 C/D dimers, with B, C, and D subunits located at the two-fold axis and the A subunits at the five-fold axis. Overall, our data showed that VP1 sequences detected several decades apart both folded into T = 4 VLPs that shared common structural features not observed in T = 3 VLPs.

2. Materials and methods

2.1. VLP and virion preparation

The full-length VP1 genes for NSW-2012 (Genebank accession number: JX459908), CHDC-1974 (ACT76142), and GII.4c (Parra et al., 2012) were cloned and expressed in a baculovirus system (Hansman et al., 2005, 2007; Koromyslova and Hansman, 2017). Additionally, a construct that contained NSW-2012 VP1/VP2 was expressed. Briefly, a bacmid containing the recombinant VP1 gene (or VP1/VP2) was transfected in Sf9 insect cells. After incubation for 5–7 days, the culture medium was collected and centrifuged for 10 min at 3,000 rpm at 4 °C. The recovered baculovirus was subsequently used to infect Hi5 insect cells. At five days post infection, the culture medium was centrifuged for 10 min at 3,000 rpm at 4 °C and then 1 h at 6,500 rpm at 4 °C. The VLPs in the supernatant were concentrated by ultracentrifugation at 35,000 rpm (Beckman Ti45 rotor) for 2 h at 4 °C and then further purified using CsCl equilibrium gradient ultracentrifugation at 35,000 rpm (Beckman SW56 rotor) for 18 h at 4 °C. To remove the CsCl, the VLPs were pelleted for 2 h at 40,000 rpm (Beckman TLA55 rotor) at 4 °C and subsequently resuspended in PBS (pH 7.4). GII.4 virions in stool were also purified using this centrifugation technique, except without the CsCl step.

2.2. Negative stain electron microscopy

The integrity of the VLPs was confirmed using negative stain EM. The VLPs were diluted 1:30 in distilled water and applied to EM grids. The grids were washed with distilled water, stained with 0.75% uranyl acetate, and the excess uranyl acetate was removed with filter paper. Virion samples were applied to EM grids, washed with water, fixed with 4% glutaraldehyde, and then stained as above. EM images were acquired on a Zeiss 910 electron microscope at 50,000 × magnification.

2.3. Cryo-EM data sample preparation and data collection

In this study, the cryo-EM structures of NSW-2012 and CHDC-1974 VLPs (i.e., VP1-alone constructs) were determined. Briefly, VLPs (3 µl) were applied to freshly glow discharged Quantifoil holey carbon support films (R1.2/1.3) and blotted for 18 s at 100% humidity and 10 °C before being plunged in liquid ethane using an FEI Mark IV Vitrobot (Thermo Fischer Scientific). Vitrified specimens were imaged on a Titan Krios microscope (Thermo Fisher scientific) operated at 300 keV. NSW-2012 micrographs were acquired with a K2 direct electron detector with Latitude S software (Gatan) at 64,000 × magnification corresponding to a pixel size of 2.27 Å/px, while CHDC-1974 micrographs were collected using a K3 direct electron detector at 64,000 × magnification, corresponding to a pixel size of 1.375 Å/px.

2.4. Cryo-EM data processing

Initially, the movies containing 16 frames for NSW-2012 and 40 frames for CHDC-1974 were motion corrected using motioncor2 software (Li et al., 2013) and defocus estimation was performed using ctffind 4.1 software (Mindell and Grigorieff, 2003). All further image-processing steps were performed using Relion 2.1 software for NSW-2012 and cryoSPARC software for CHDC-1974 (Scheres, 2012; Punjani et al., 2017). An initial set of 1,000 particles was manually picked for 2D classification, to produce averages suitable as references for automated particle picking. The autopicked particles were sorted in a 2D classification step and the best particles were used for calculation of an initial starting model, followed by 3D classification. A subset of particles (10,548 particles) that generated the highest resolution was selected for further refinement. For NSW-2012 T = 4 VLPs, 3D refinement with icosahedral I2 symmetry imposed produced a final map at 7.3 Å and 8.2 Å resolution using Fourier Shell Correlation (FSC) cut-off at 0.143 and 0.5, respectively. Native-sized NSW-2012 T = 3 particles also were manually picked and sorted in 2D classification. In total, 391 particles were selected for further 3D structure determination. Refinement of these NSW-2012 T = 3 particles yielded a map of 15 Å and 19 Å resolution using FSC cut-off at 0.143 and 0.5, respectively. For CHDC-1974, a subset of 42,485 particles for refinement led to the calculation of a map at 6.1 Å and 7.2 Å resolution for FSC cut-off at 0.143 and 0.5, respectively. The cryo-EM T = 4 VLP structures for CHDC-1974 (accession number: EMD-4549) and NSW-2012 (EMD-4550) were deposited at EMDB. The cryo-EM VLP structure for NSW-2012 with T = 3 icosahedral symmetry is available on request.

2.5. Fitting of the X-ray structures into the density maps

X-ray crystal structures of NSW-2012 P domain (4OOS) and CHDC-1974 P domain (5IYN) were fitted into the respective densities using the “fit in map” command in the UCSF Chimera software (Pettersen et al., 2004). Since a high-resolution GII.4 shell domain structure was unavailable, the GI.1 Norwalk virus S domain was extracted from the X-ray crystal structure (1IHM) and fitted into the GII.4 cryo-EM densities using both UCSF Chimera software command "fit in map" and manual adjustment.

3. Results

The purpose of this study was to analyze GII.4 VLP architecture of two genetic GII.4 variants detected in 1974 and 2012 (CHDC-1974 and NSW-2012, respectively). Compared to CHDC-1974, NSW-2012 VP1 sequence had a single amino acid insertion at position 394 (NSW-2012 numbering) (Fig. 1). NSW-2012 and CHDC-1974 shared 89% amino acid identity, with most (45 of 54) amino acid substitutions in the P domain.

Negative stain EM images revealed that NSW-2012 and CHDC-1974 VLPs (VP1-alone constructs) exhibited the characteristic norovirus

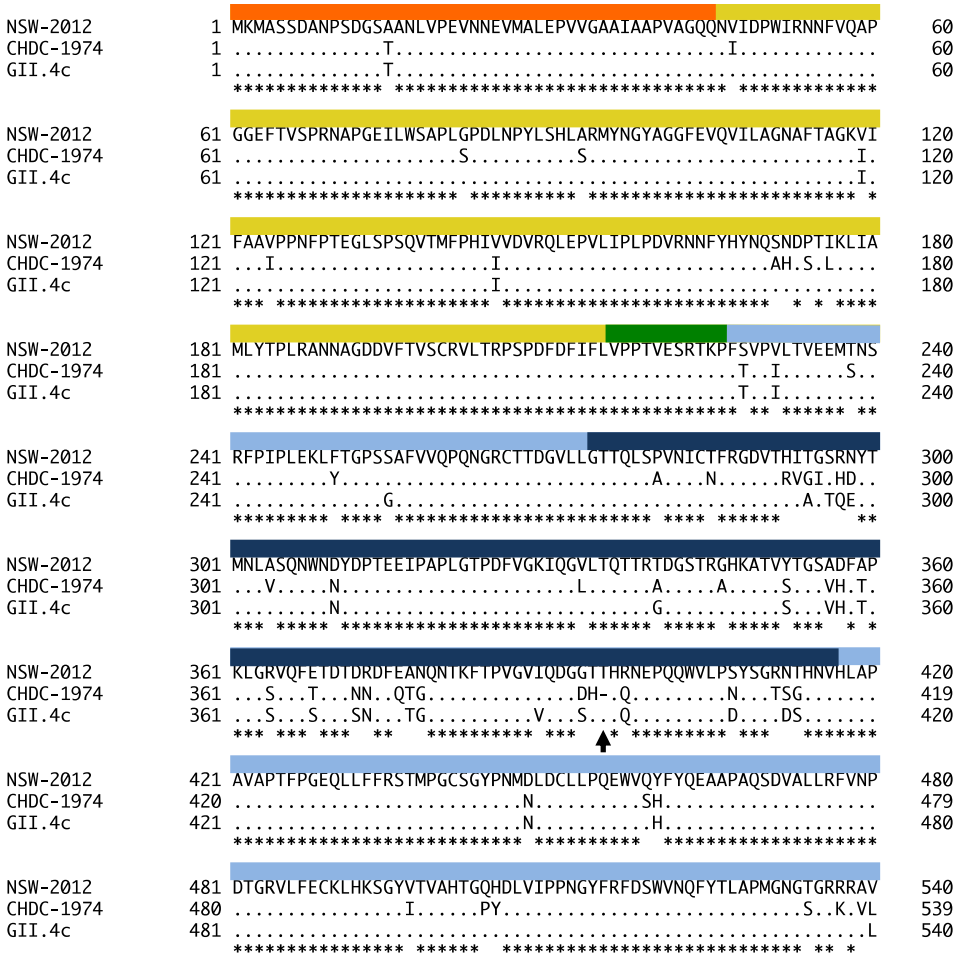

Fig. 1. Amino acid sequence alignment of GII.4 VP1. NSW-2012 (JX459908), CHDC-1974 (ACT76142), and GII.4c (Parra et al., 2012) VP1 amino acid sequences were aligned using ClustalX. The VP1 N-terminus and S domain (orange/yellow), hinge region (green), P1 subdomain (light blue), and P2 subdomain (navy) were labeled accordingly. Compared to CHDC-1974, NSW-2012 and GII.4c VP1 had a single amino acid insertion (arrow) at position 394 (NSW-2012 numbering). The S domain and hinge region were mainly conserved, whereas most amino acid substitutions were located in the P2 subdomain.

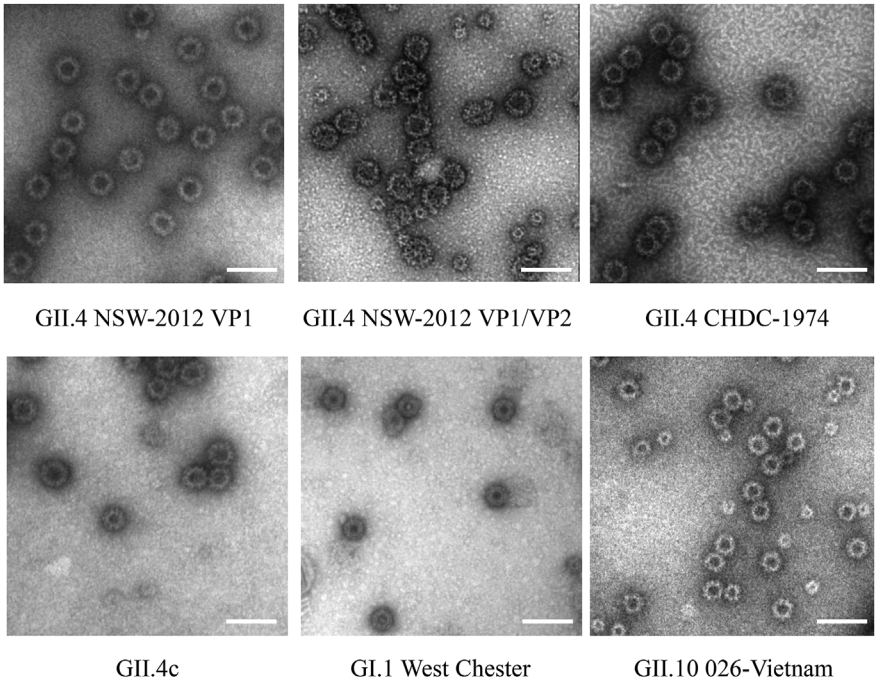

Fig. 2. EM images of GI and GII VLPs. Negative stain EM images of norovirus VLPs show the characteristic norovirus morphology (50,000 × magnification). The diameter of the CHDC-1974 and NSW-2012 VLPs (VP1-alone construct) was ~52 nm. The diameter of GI.1 West Chester (AY502016.1) and GII.10 Vietnam026 (AF504671) VLPs were ~38 nm and ~43 nm, respectively. NSW-2012 VP1/VP2 formed VLPs that were ~52 nm and ~26 nm in diameter. The diameter of GII.4c was ~52 and ~45 nm. The bar represents 100 nm.

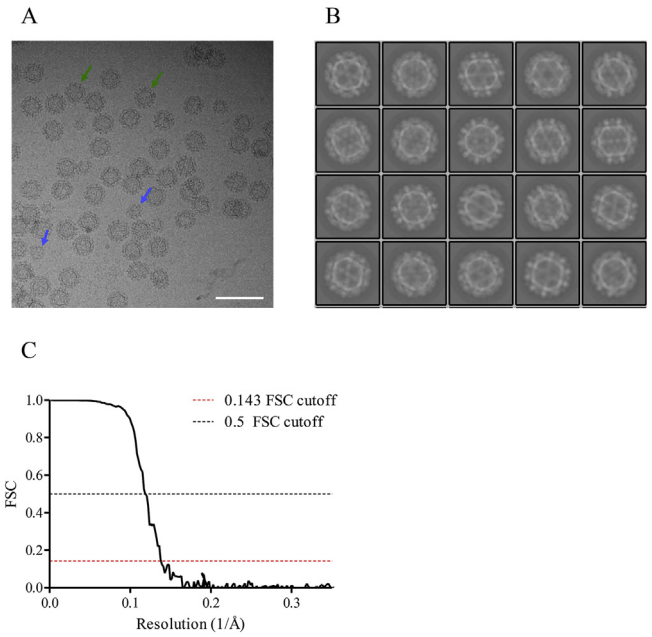

Fig. 3. NSW-2012 cryo-EM data processing. (A) A representative cryo-EM micrograph of NSW-2012 VLPs at 64,000 × magnification. The blue and green arrows show examples of VLPs measuring ~46 nm and ~50 nm, respectively. The scale bar represents 100 nm. (B) 2D classification of GII.4 NSW-2012 T = 4 VLPs. (C) FSC plot of the icosahedral reconstruction of NSW-2012 indicates a resolution of 7.3 Å and 8.2 Å resolution using FSC cut-off at 0.143 and 0.5, respectively.

morphology, i.e., P dimer spikes on the surface (Fig. 2). However, the diameter of these VLPs was ~52 nm, which was larger than GII.10 and GI.1 VLPs that had diameters of ~43 nm and ~38 nm, respectively. An expression construct that contained NSW-2012 VP1/VP2 also formed these larger VLPs (~52 nm in diameter), as well as smaller VLPs, ~26 nm in diameter. The GII.4c VP1 produced VLPs that had diameters of ~52 and ~45 nm. Overall, these data indicated that GII.4 VP1 produced at least three types of VLPs, i.e., ~52 nm, ~45 nm, and ~26 nm in diameter. Following these results, we proceeded to determine the structures of CHDC-1974 and NSW-2012 VLPs (i.e., VP1-alone constructs).

3.1. Cryo-EM structure of NSW-2012 T = 4 VLPs

The structure of the NSW-2012 VLPs was determined using cryo-EM and 3D icosahedral image reconstruction. These VLPs were mono-disperse in vitreous ice and appeared mostly homogenous in size (Fig. 3A and B). From 364 images, 10,548 particles were used for final image reconstruction (Fig. 3C). Surprisingly, NSW-2012 VLPs had a T = 4 icosahedral symmetry (Fig. 4A). This also revealed that these VLPs were composed of 240 copies of VP1, rather than 180 copies, as found in other caliciviruses. The inner diameter of the T = 4 shell was 32 nm, whereas the outer capsid diameter was 50 nm. The shell volume of the T = 4 VLPs was ~12,724 nm^3, which was ~2.1 × (~5,985 nm^3) the volume of the GII.10 T = 3 VLPs that had an inner shell diameter of 23 nm.

Structural analysis of the T = 4 VLPs indicated that VP1 adopted four quasi-equivalent conformations, termed A, B, C, and D. These four conformations formed two distinct dimer classes: A/B and C/D (Fig. 4B and C). The B, C, and D subunits alternated about the two-fold symmetry axis, while the A subunit was positioned at the five-fold axis (Fig. 4). The T = 4 VLPs were composed of 60 A/B dimers and 60 C/D dimers, which was distinct from the T = 3 VLPs that have been shown to be assembled from 60 A/B and 30 C/C dimers. We also observed that both A/B and C/D dimers had a convex S domain conformation, which

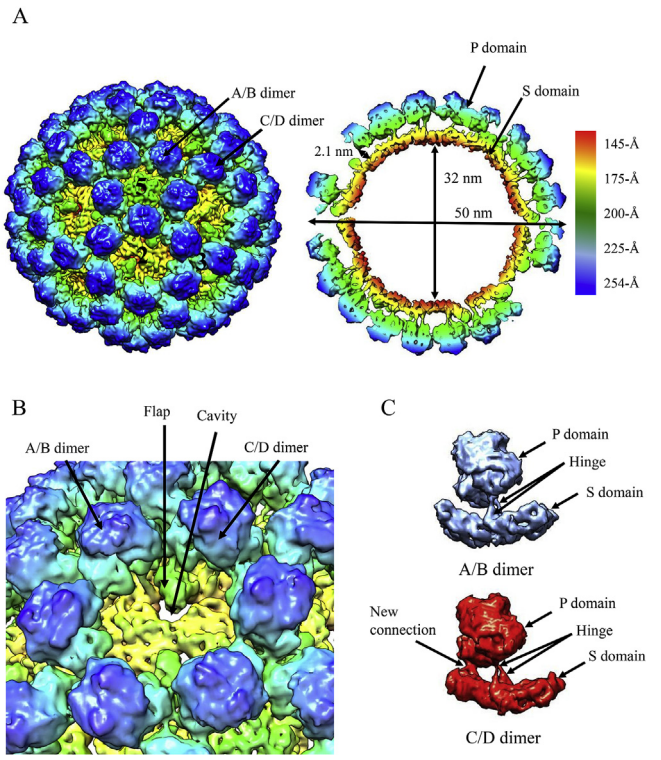

Fig. 4. Cryo-EM reconstruction structure of NSW-2012 T = 4 VLPs shows several new structural features. (A) The left side shows that NSW-2012 VLPs have a T = 4 icosahedral symmetry (symmetry axes labeled 2, 3 and 5). These VLPs were composed of 240 copies of VP1 and VP1 adopted four quasiequivalent conformations (A, B, C, and D) that gave rise to two distinct dimers (A/B and C/D). At the icosahedral two-fold axis, the B, C, and D subunits were alternating, while the A subunits are positioned at the five-fold axis. The right side shows a cutaway section of these VLPs and indicates that the inner and outer diameters are 32 nm and 50 nm, respectively. The P domains are elevated ~21 Å off the S domain. (B) The cavity and flap-like structures are observed on opposing sides at the two-fold axis and are associated with the S domain on the D subunit. (C) NSW-2012 T = 4 VLPs are formed with 60 A/B and 60 C/D VP1 dimers. The A/B and C/D dimers show an equivalent convex conformation of the S domain. An additional connection was also observed between the D subunit of the S and P domain.

was in contrast to GI.1 VLPs that consisted of both convex (A/B) and flat (C/C) dimers (Prasad et al., 1999).

Apart from this major structural change, the T = 4 VLPs had several other novel structural features. Typically, calicivirus S domains form a contiguously closed capsid. In the case of the T = 4 VLPs, a small cavity and flap-like structure disrupting the contiguous shell was observed (Figs. 4B and 5A). This feature was associated with the S domain of the D subunit and found on opposing sides at the two-fold axis. We also found that the P domain on the T = 4 VLPs was elevated 21 Å off the shell by an extended hinge region (Figs. 4 and 5B). In fact, this distance was higher than the P domains on the GII.10 VLPs, which were raised ~14 Å (Hansman et al., 2012).

In order to better understand how VP1 folded in these T = 4 VLPs, the X-ray crystal structures of the T = 3 GI.1 S domain (1IHM) and NSW-2012 P domain (4OOS) were fitted into the T = 4 VLP density map (Fig. 5A). For the S domain, the orientation of the T = 4 A/B/C subunits was comparable to the S domain of the GI.1 A/B/C subunits at the five-fold and three-fold axes of the T = 3 particle. For T = 4 D subunit, the GI.1 C subunit was manually shifted to fit the T = 4 VLP S domain density. The resulting (upward) shift of this subunit was directly associated with the formation of the small cavity and flap-like structure. In the case of the P domains, the NSW-2012 P domain X-ray crystal structure unambiguously fitted into T = 4 A/B and C/D dimers,

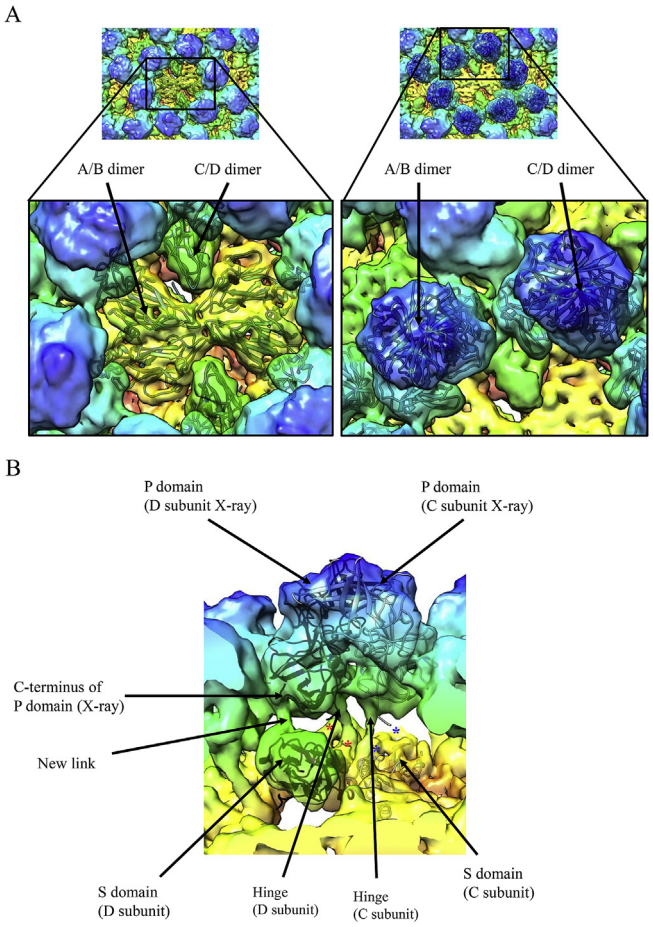

Fig. 5. The X-ray crystal structures of NSW-2012 P domain and GI.1 S domain were fitted into the T = 4 VLP density map. (A) Left shows the X-ray crystal structure of the GI.1 S domain (1IHM, cartoon) fitted into the A/B and C/D S domain densities. Right shows the X-ray crystal structure of NSW-2012 P domain (4OOS, cartoon) fitted into the A/B and C/D P domain dimers (B) Close-up view of an NSW-2012 C/D dimer. The new connection between the S domain and the C-terminus of the P domain is shown. The asterisk represents the missing hinge region on the X-ray crystal structures that connects of the S and P domains for the C subunit (blue) and D subunit (red).

with a cross correlation coefficient of 0.96. Interestingly, an apparent new point of contact was also observed on the D subunit between the S domain and the C-terminus on the P domain (Fig. 5B).

3.2. Cryo-EM structure of NSW-2012 T = 3 VLPs

As mentioned, the structure of the NSW-2012 T = 4 VLPs was determined from 10,548 particles. However, a very small subset of particles (391 particles) appeared native-sized (Fig. 3A). Reconstruction of these particles revealed VLPs with a T = 3 icosahedral symmetry and a diameter of ~46 nm (Fig. 6C). Based on this geometry, the VLPs were likely composed of 180 copies of VP1.

Not surprisingly, the GII.4 T = 3 VLPs appeared more similar to the GII.10 T = 3 VLPs than the GI.1 T = 3 VLPs. For example, a gap existed between S and P domain, which indicated that these NSW-2012 P domains were also raised off the S domain, although the hinge region could not be resolved. Improving the resolution of these VLPs is currently challenging, since only a small percentage of T = 3 particles were assembled and particle size separation using CsCl and sucrose gradient ultracentrifugation remains difficult. Interestingly, the cavity and flap-like structure found on the T = 4 VLPs was not observed on these T = 3 VLPs.

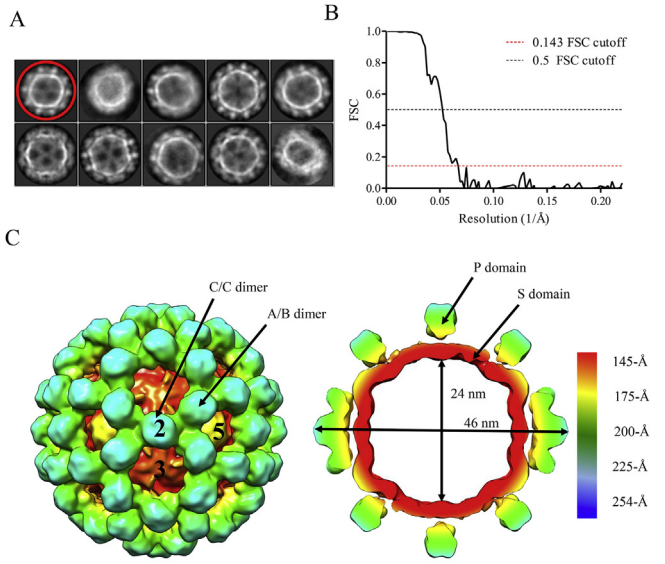

Fig. 6. Cryo-EM reconstruction structure of NSW-2012 T = 3 VLPs. (A) 2D classification of 1,780 manually picked particles. The first class (red circle) shows particles of a smaller diameter compared to other class averages. These smaller particles were used for further refinement. (B) FSC plot of the icosahedral reconstruction of T = 3 VLPs indicates a resolution of 15 Å and 19 Å resolution using FSC cut-off at 0.143 and 0.5, respectively. (C) The left side shows NSW-2012 VLPs exhibiting T = 3 icosahedral symmetry (symmetry axes labeled 2, 3, and 5). These VLPs were composed of 180 copies of VP1 that form A/B and C/C dimers. The cutaway section (right) shows the inner and outer diameter of the particle, which measured 24 and 46 nm, respectively. At this resolution the hinge region could not be resolved, but the large gap between S and P domain indicates that the P domains are raised up from the shell.

Overall, these results indicated that NSW-2012 VP1 could form both T = 3 and T = 4 particles, but only ~5% of the population (391 of 10,548) were native-sized. This smaller proportion of T = 3 VLPs was also observed with several VLP preparations.

3.3. Cryo-EM structure of GII.4 CHDC-1974 T = 4 VLPs

To test whether assembly of VLPs with T = 4 icosahedral symmetry is a property of other GII.4 norovirus variants, we proceeded to determine the cryo-EM structure of VLPs produced by VP1 of CHDC-1974. These VLPs were mostly mono-disperse and homogenous in size (Fig. 7A). From 591 images, 42,485 particles were used for final 3D reconstruction (Fig. 7B and C). Interestingly, we discovered that the CHDC-1974 VLPs also had T = 4 symmetry (Fig. 8A).

In general, CHDC-1974 VLPs closely resembled those of NSW-2012. We found that CHDC-1974 T = 4 VLPs were composed of 240 copies of VP1 that formed the quasi-equivalent subunits A, B, C, and D, with A/B and C/D dimeric capsomeres. The inner diameter of the shell was 32 nm, whereas the outer diameter of the capsid was 50 nm. As in NSW-2012 VLPs, cavity and flap-like structures were also present on the CHDC-1974 VLPs (Fig. 8B). The CHDC-1974 A/B and C/D dimers showed a similar convex conformation as NSW-2012 dimers, although slightly less pronounced (Fig. 8C).

We also evaluated how the X-ray crystal structure of the GI.1 S domain (1IHM) and CHDC-1974 P domain (5IYN) fitted into the CHDC-1974 VLP density map (Fig. 9A). Similar to NSW-2012 VLPs, the GI.1 S domain could be easily positioned into the density of the CHDC-1974 VLP A, B, and C subunits, whereas the GI.1 S domain needed to be manually positioned in order to occupy the CHDC-1974 VLP D subunit density. The X-ray crystal structure of CHDC-1974 P domain nicely fitted into the A/B/C/D subunits on the CHDC-1974 VLP density map. Similar to NSW-2012 VLPs, the CHDC-1974 VLP P domains were also raised ~21 Å off the shell domain (Fig. 8A, C, and 9B). Moreover, a

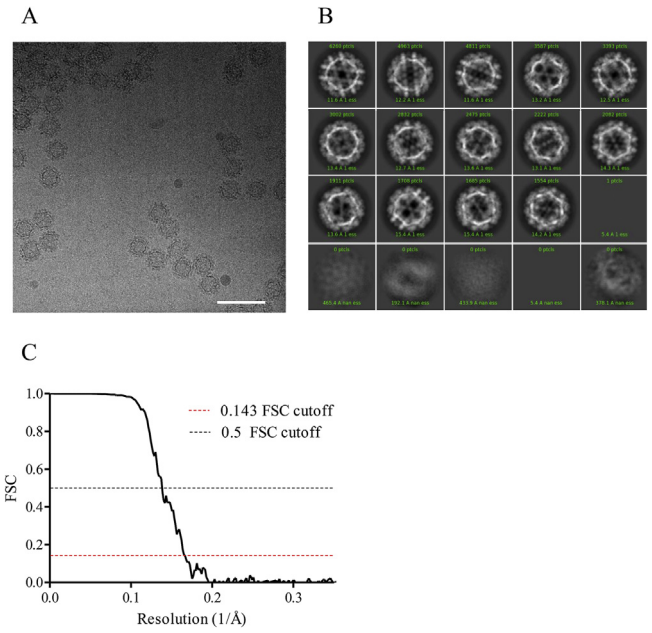

Fig. 7. CHDC-1974 cryo-EM data processing. (A) A representative cryo-EM micrograph of CHDC-1974 VLPs at 64,000 × magnification. The scale bar represents 100 nm. (B) 2D classification of CHDC-1974 particles. (C) FSC plot of the icosahedral reconstruction of CHDC-1974 indicates a resolution of 6.1 Å and 7.2 Å resolution using FSC cut-off at 0.143 and 0.5, respectively.

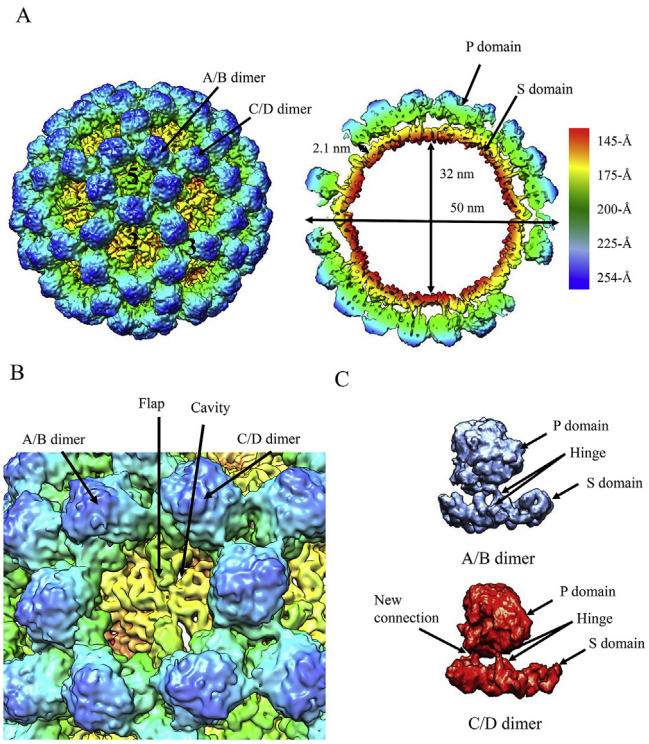

Fig. 8. Cryo-EM structure and analysis of CHDC-1974 VLPs. The image on the left side shows that CHDC-1974 VLPs have a T = 4 icosahedral symmetry (symmetry axes labeled 2, 3 and 5) and are composed of 240 copies of VP1. The VP1 exhibited four quasiequivalent conformations (A, B, C, and D) that gave rise to two distinct dimers (A/B and C/D). At the icosahedral two-fold axis, the B, C, and D subunits were alternating, while the A subunit was located around the five-fold axis. The right side shows a cutaway section of these VLPs and indicates that the inner and outer diameters are 32 nm and 50 nm, respectively. The P domains are elevated ~2.1 nm off the S domain. (B) The cavity and flap-like structures are observed at the two-fold axis and are found on opposing sides. The cavity and flap-like structures are associated with the S domain on the D subunit. (C) The A/B and C/D dimers show an equivalent convex conformation on the S domain. Also, the additional connection between the D subunit of the S and P domain was found on the CHDC-1974 T = 4 VLPs.

similar contact interface was observed between the CHDC-1974 VLP S and P domains on the D subunit. Overall, these results clearly showed that NSW-2012 and CHDC-1974 T = 4 VLPs were structurally similar. However, unlike NSW-2012, CHDC-1974 T = 3 VLPs were not observed in the cryo-EM images.

3.4. Negative stain EM of GII.4 virions

To test whether GII.4 virions assembled into T = 3 or T = 4 particles, we used negative stain EM of authentic GII.4 virions. These virion images revealed particles with a smaller diameter of ~44 nm compared to the T = 4 VLPs (~50 nm) (Fig. 10). This size corresponds to the diameter determined for the NSW-2012 T = 3 VLPs and indicates that GII.4 virions likely exhibit T = 3 icosahedral symmetry.

4. Discussion

In our study presented here, we have shown that upon heterologous expression of human norovirus GII.4 VP1 in insect cells, VLPs are formed that mostly adopt a T = 4 icosahedral symmetry. More importantly, our results showed that GII.4 VP1 sequences isolated over three decades apart remained structurally conserved. This could imply that other GII.4 VP1 sequences also form T = 4 VLPs when expressed in insect cells, especially since these two sequences had only 89% amino acid identity.

Our findings are at odds with the likely T = 3 symmetry encoded by the GII.4 virion. However, it is possible that VP1 undergoes different post-translational modifications in insect cells, compared to expression in mammalian host cells, and these modifications could ultimately cause the differences in symmetry. Furthermore, it is also possible that interaction with the RNA facilitates the assembly of T = 3 particles and absence of RNA in the insect cell expression system favors assembly of T = 4 particles. However, as VLPs of other norovirus genotypes form T = 3 particles in insect cells, it appears as if this formation of the T = 4 particles is GII.4-specific. Nevertheless, our results show that it cannot be routinely assumed that all norovirus VLPs are identical to authentic T = 3 virions and cautious examination of VLPs in EM images is important.

Next to the symmetry difference, the T = 4 particles also exhibited other distinct structures features, in particular the cavity and flap-like structure that disrupted the contiguous shell. The cavity and flap-like structure may arise as a consequence of the C/D dimer having a strongly pronounced curvature, thereby preventing the S-domain from forming the expected contacts with neighboring B- and C-type subunits. Ultimately, this might lead to a decrease in contact interface between adjacent S domain subunits. Alternatively, there might be insufficient space to allow the D subunit S-domain to pack such that it lies in the plane of the shell without causing steric collision with neighboring subunits.

We also observed a new connection between the C-terminus of the D-subunit and the corresponding S domain. This contact might stabilize the convex conformation of the C/D dimer and therefore could be associated with the formation of the small cavity and flap-like structure. Indeed, the C-terminus of VP1 on the GI.1 VLPs and the GII.4 P domain were previously found to be flexible (Prasad et al., 1999; Singh et al., 2015) and was shown to be important for the size and stability of VLPs (Bertolotti-Ciarlet et al., 2002). This suggests that the flexibility of the C-terminus might also regulate the assembly of differently sized particles.

Another structural feature of the T = 4 VLPs was the extended P domains. The T = 4 P domains were raised 21 Å off the shell, which

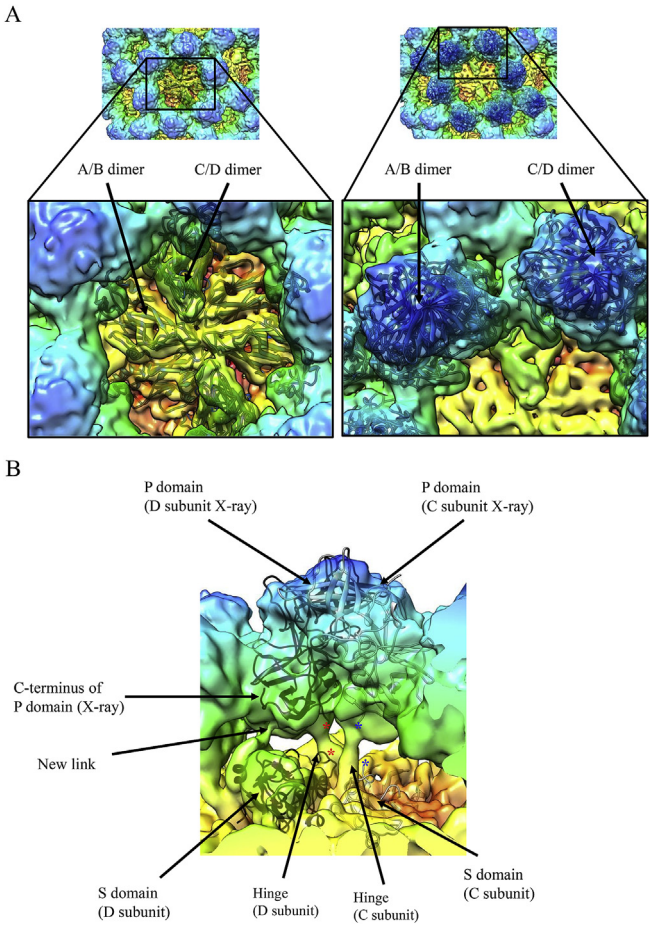

Fig. 9. The X-ray crystal structures of CHDC-1974 P domain and GI.1 S domain were fitted into the VLP density map. (A) Left shows the X-ray crystal structure of the GI.1 S domain (1IHM, cartoon) fitted into the A/B and C/D S domain dimers. Right shows the X-ray crystal structure of NSW-2012 P domain (5IYN, cartoon) fitted into the A/B and C/D P domain dimer densities. (B) Close-up view of CHDC-1974 C/D dimer. The new connection between the S domain and the C-terminus of the P domain is shown. The asterisk represents the missing hinge region on the X-ray crystal structures that connects of the S and P domains for the C subunit (blue) and D subunit (red).

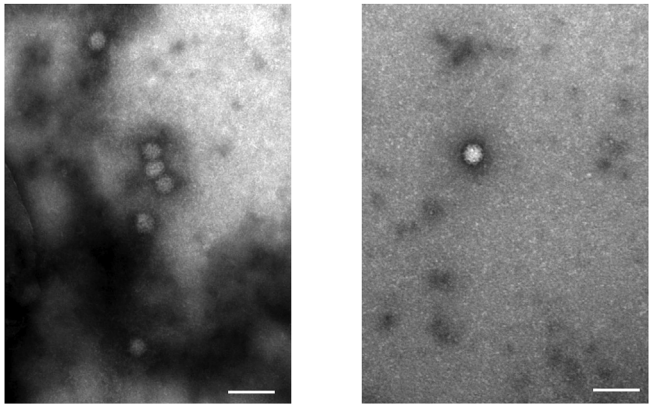

Fig. 10. EM images of GII.4 virions. Negative stain EM images of GII.4 virions show that the virions exhibit a smaller diameter (~44 nm) than the T = 4 VLPs expressed in insect cells that were ~52 nm (see Fig. 2).

was notably more than for the GII.10 VLPs, where the P domains were raised ~14 Å (Hansman et al., 2012). Interestingly, the hinge regions in NSW-2012 and GII.10 were both ~10 amino acids in length, and mainly conserved (Hansman et al., 2012; Koromyslova and Hansman, 2015). This suggests that the extent to which the hinge region was raised could be independent of the amino acid sequence. Yet, the raised P domains appear to be a common feature for GII noroviruses. Clearly, additional studies are needed to better understand the extension mechanism(s) and purpose of the extended P domains.

The GII.4 VLPs and/or their corresponding P domains have been extensively studied using ELISA and X-ray crystallography (Kilic et al., 2019; Koromyslova and Hansman, 2015, 2017; Singh et al., 2015; Koromyslova et al., 2018; Doerflinger et al., 2016). We found that the NSW-2012 P domains were capable of binding numerous HBGA types and the VLPs cross-reacted with Nanobodies and antibodies that were raised against other genotypes or GII.4 variants. NSW-2012 VLPs did not bind bile acid and poorly bound human milk oligosaccharides (HMOs), but this finding was also observed with other GII.4 VLPs. Overall, our studies show that these T = 4 VLPs were biologically functional and structurally comparable to other T = 3 VLPs.

Norovirus vaccines that are currently tested in clinical trials use a combination of VLPs, including the GII.4c VLPs (Parra et al., 2012; Treanor et al., 2014). Sequence analysis of GII.4c and NSW-2012 VP1 showed 94% amino acid identity, with most substitutions (28 of 31) located in the P domain (Fig. 1). Not surprisingly, the insect cell-expressed GII.4c VP1 also produced VLPs that had diameters of ~52 and ~45 nm. Further structural studies of the GII.4c VLPs are highly anticipated.

In general, studies on norovirus vaccines have shown that norovirus-specific antibody titers were raised after vaccination with VLPs, but the levels of protection were not strongly improved compared to placebo groups (Bernstein et al., 2015). This might indicate that vaccination leads to production of neutralizing antibodies against epitopes on T = 4 VLPs that are not accessible on T = 3 virions (i.e., when challenged) and that therefore vaccine efficacy could be lowered by a sub-optimal antigen. Moreover, a recent follow-up study on the norovirus VLP vaccine showed that even though seroresponse stayed above the baseline, Pan-Ig, IgA, and HBGA blocking antibodies waned in the course of a year after vaccination and that the HBGA blocking responses to a memory probe after 365 days for GII.4c VLPs did not show characteristics of immune memory (Atmar et al., 2019).

In summary, there are two rather important consequences of our novel results. Firstly, the GII.4 VLPs appeared to be morphologically similar to other norovirus VLPs in negative stain EM, but were in fact mainly larger and exhibiting T = 4 symmetry. Consequently, GII.4 VLPs could be composed of either 180 or 240 copies of VP1, which might impact on studies where GII.4 VLPs were assumed to be composed of T = 3 particles. Secondly, GII.4 vaccines might contain a mixture of T = 3 and T = 4 VLPs. Therefore, it will be important to investigate how these differently sized particles might influence vaccine trials, considering that the native virion has a T = 3 symmetry.

Acknowledgements

We would like to acknowledge the microscopy support from the Cryo-EM network of Heidelberg University; the EM core facility at DKFZ; the state of Baden-Württemberg with the High Performance Cluster (bwHPC); and the German Research Foundation (INST 35/1134-1 FUGG). The authors further acknowledge the data storage service (SDS@hd) by the ministry of Science, Research and the Arts Baden-Wuerttemberg (MWK) and the German Research Foundation (INST 35/1314-1 FUGG.) We thank Anna Koromyslova for EM images of GII.4 virions and Benedikt Wimmer for setting up the cryo-EM software. The funding for this study was provided by the CHS foundation; the Baden-Württemberg Stiftung (GLYCAN-BASED ANTIVIRAL AGENTS); Deutsche Forschungsgemeinschaft (DFG, FOR2327); and the BMBF VIP + (Federal Ministry of Education and Research) (NATION, 03VP00912). David Bhella is supported by the United Kingdom Medical Research Council (MC_UU_12014/7).

References

Ajami, N.J., Barry, M.A., Carrillo, B., Muhaxhiri, Z., Neill, F.H., Prasad, B.V., Opekun, A.R., Gilger, M.A., Graham, D.Y., Atmar, R.L., Estes, M.K., 2012. Antibody responses to norovirus genogroup GI.1 and GII.4 proteases in volunteers administered Norwalk virus. Clin. Vaccine Immunol. 19, 1980–1983.

Atmar, R.L., Baehner, F., Cramer, J.P., Lloyd, E., Sherwood, J., Borkowski, A., Mendelman Paul, M., 2019. Antibody persistence to two Virus-Like Particle norovirus vaccine candidate formulations in healthy adults: one-year follow-up with memory probe vaccination. J. Infect. Dis. https://doi.org/10.1093/infdis/jiz170.

Baric, R.S., Yount, B., Lindesmith, L., Harrington, P.R., Greene, S.R., Tseng, F.C., Davis, N., Johnston, R.E., Klapper, D.G., Moe, C.L., 2002. Expression and self-assembly of norwalk virus capsid protein from venezuelan equine encephalitis virus replicons. J. Virol. 76, 3023–3030.

Bernstein, D.I., Atmar, R.L., Lyon, G.M., Treanor, J.J., Chen, W.H., Jiang, X., Vinje, J., Gregoricus, N., Frenck Jr., R.W., Moe, C.L., Al-Ibrahim, M.S., Barrett, J., Ferreira, J., Estes, M.K., Graham, D.Y., Goodwin, R., Borkowski, A., Clemens, R., Mendelman, P.M., 2015. Norovirus vaccine against experimental human GII.4 virus illness: a challenge study in healthy adults. J. Infect. Dis. 211, 870–878.

Bertolotti-Ciarlet, A., White, L.J., Chen, R., Prasad, B.V., Estes, M.K., 2002. Structural requirements for the assembly of Norwalk virus-like particles. J. Virol. 76, 4044–4055.

Bhella, D., Goodfellow, I.G., 2011. The cryo-electron microscopy structure of feline calicivirus bound to junctional adhesion molecule A at 9-angstrom resolution reveals receptor-induced flexibility and two distinct conformational changes in the capsid protein VP1. J. Virol. 85, 11381–11390.

Bok, K., Abente, E.J., Realpe-Quintero, M., Mitra, T., Sosnovtsev, S.V., Kapikian, A.Z., Green, K.Y., 2009. Evolutionary dynamics of GII.4 noroviruses over a 34-year period. J. Virol. 83, 11890–11901.

Chen, R., Neill, J.D., Noel, J.S., Hutson, A.M., Glass, R.I., Estes, M.K., Prasad, B.V., 2004. Inter- and intragenus structural variations in caliciviruses and their functional implications. J. Virol. 78, 6469–6479.

Conley, M., Emmott, E., Orton, R., Taylor, D., Carneiro, D.G., Murata, K., Goodfellow, I.G., Hansman, G.S., Bhella, D., 2017. Vesivirus 2117 capsids more closely resemble sapovirus and lagovirus particles than other known vesivirus structures. J. Gen. Virol. 98, 68–76.

Doerflinger, S.Y., Tabatabai, J., Schnitzler, P., Farah, C., Rameil, S., Sander, P., Koromyslova, A., Hansman, G.S., 2016. Development of a nanobody-based lateral flow immunoassay for detection of human norovirus. mSphere 1.

Donaldson, E.F., Lindesmith, L.C., Lobue, A.D., Baric, R.S., 2008. Norovirus pathogenesis: mechanisms of persistence and immune evasion in human populations. Immunol. Rev. 225, 190–211.

Eden, J.S., Tanaka, M.M., Boni, M.F., Rawlinson, W.D., White, P.A., 2013. Recombination within the pandemic norovirus GII.4 lineage. J. Virol. 87, 6270–6282.

Ettayebi, K., Crawford, S.E., Murakami, K., Broughman, J.R., Karandikar, U., Tenge, V.R., Neill, F.H., Blutt, S.E., Zeng, X.L., Qu, L., Kou, B., Opekun, A.R., Burrin, D., Graham, D.Y., Ramani, S., Atmar, R.L., Estes, M.K., 2016. Replication of human noroviruses in stem cell-derived human enteroids. Science 353, 1387–1393.

Hansman, G.S., Natori, K., Oka, T., Ogawa, S., Tanaka, K., Nagata, N., Ushijima, H., Takeda, N., Katayama, K., 2005. Cross-reactivity among sapovirus recombinant capsid proteins. Arch. Virol. 150, 21–36.

Hansman, G.S., Natori, K., Shirato-Horikoshi, H., Ogawa, S., Oka, T., Katayama, K., Tanaka, T., Miyoshi, T., Sakae, K., Kobayashi, S., Shinohara, M., Uchida, K., Sakurai, N., Shinozaki, K., Okada, M., Seto, Y., Kamata, K., Nagata, N., Tanaka, K., Miyamura, T., Takeda, N., 2006. Genetic and antigenic diversity among noroviruses. J. Gen. Virol. 87, 909–919.

Hansman, G.S., Saito, H., Shibata, C., Ishizuka, S., Oseto, M., Oka, T., Takeda, N., 2007. Outbreak of gastroenteritis due to sapovirus. J. Clin. Microbiol. 45, 1347–1349.

Hansman, G.S., Taylor, D.W., McLellan, J.S., Smith, T.J., Georgiev, I., Tame, J.R., Park, S.Y., Yamazaki, M., Gondaira, F., Miki, M., Katayama, K., Murata, K., Kwong, P.D., 2012. Structural basis for broad detection of genogroup II noroviruses by a monoclonal antibody that binds to a site occluded in the viral particle. J. Virol. 86, 3635–3646.

Hutson, A.M., Atmar, Robert L., Graham, David Y., Estes, Mary K., 2002. Norwalk virus infection and disease is associated with ABO histo-blood group type. JID (J. Infect. Dis.) 185, 1335–1337.

Jones, M.K., Watanabe, M., Zhu, S., Graves, C.L., Keyes, L.R., Grau, K.R., Gonzalez-Hernandez, M.B., Iovine, N.M., Wobus, C.E., Vinje, J., Tibbetts, S.A., Wallet, S.M., Karst, S.M., 2014. Enteric bacteria promote human and mouse norovirus infection of B cells. Science 346, 755–759.

Kilic, T., Koromyslova, A., Hansman, G.S., 2019. Structural basis for human norovirus capsid binding to bile acids. J. Virol. 93.

Koromyslova, A.D., Hansman, G.S., 2015. Nanobody binding to a conserved epitope promotes norovirus particle disassembly. J. Virol. 89, 2718–2730.

Koromyslova, A.D., Hansman, G.S., 2017. Nanobodies targeting norovirus capsid reveal functional epitopes and potential mechanisms of neutralization. PLoS Pathog. 13, e1006636.

Koromyslova, A.D., Morozov, V.A., Hefele, L., Hansman, G.S., 2018. Human norovirus neutralized by a monoclonal antibody targeting the HBGA pocket. J. Virol. https://doi.org/10.1128/JVI.02174-18.

Lawton, J.A., Zeng, C.Q., Mukherjee, S.K., Cohen, J., Estes, M.K., Prasad, B.V., 1997. Three-dimensional structural analysis of recombinant rotavirus-like particles with intact and amino-terminal-deleted VP2: implications for the architecture of the VP2 capsid layer. J. Virol. 71, 7353–7360.

Li, X., Mooney, P., Zheng, S., Booth, C., Braunfeld, M.B., Gubbens, S., Agard, D.A., Cheng, Y., 2013. Electron counting and beam-induced motion correction enable near atomic resolution single particle cryoEM. Nat. Methods 10, 584–590.

Lindesmith, L.C., Donaldson, E.F., Baric, R.S., 2011. Norovirus GII.4 strain antigenic variation. J. Virol. 85, 231–242.

Lindesmith, L.C., Debbink, K., Swanstrom, J., Vinje, J., Costantini, V., Baric, R.S., Donaldson, E.F., 2012. Monoclonal antibody-based antigenic mapping of norovirus GII.4-2002. J. Virol. 86, 873–883.

Lindesmith, L.C., Costantini, V., Swanstrom, J., Debbink, K., Donaldson, E.F., Vinje, J., Baric, R.S., 2013. Emergence of a norovirus GII.4 strain correlates with changes in evolving blockade epitopes. J. Virol. 87, 2803–2813.

Marionneau, S., Ruvoën, N., Le Moullac, Vaidye, B., Clement, M., Cailleau–Thomas, A., Ruiz–Palacois, G., Huang, P., Jiang, X., Le Pendu, J., 2002. Norwalk virus binds to histo-blood group antigens present on gastroduodenal epithelial cells of secretor individuals. Gastroenterology 122, 1967–1977.

Mindell, J.A., Grigorieff, N., 2003. Accurate determination of local defocus and specimen tilt in electron microscopy. J. Struct. Biol. 142, 334–347.

Parra, G.I., Bok, K., Taylor, R., Haynes, J.R., Sosnovtsev, S.V., Richardson, C., Green, K.Y., 2012. Immunogenicity and specificity of norovirus Consensus GII.4 virus-like particles in monovalent and bivalent vaccine formulations. Vaccine 30, 3580–3586.

Pettersen, E.F., Goddard, T.D., Huang, C.C., Couch, G.S., Greenblatt, D.M., Meng, E.C., Ferrin, T.E., 2004. UCSF Chimera–a visualization system for exploratory research and analysis. J. Comput. Chem. 25, 1605–1612.

Prasad, B.V.V., Schmid, M.F., 2012. Principles of virus structural organization. Adv. Exp. Med. Biol. 726, 17–47.

Prasad, B.V., Rothnagel, R., Jiang, X., Estes, M.K., 1994. Three-dimensional structure of baculovirus-expressed Norwalk virus capsids. J. Virol. 68, 5117–5125.

Prasad, B.V., Hardy, M.E., Dokland, T., Bella, J., Rossmann, M.G., Estes, M.K., 1999. X-ray crystallographic structure of the Norwalk virus capsid. Science 286, 287–290.

Punjani, A., Rubinstein, J.L., Fleet, D.J., Brubaker, M.A., 2017. cryoSPARC: algorithms for rapid unsupervised cryo-EM structure determination. Nat. Methods 14, 290–296.

Ramani, S., Atmar, R.L., Estes, M.K., 2014. Epidemiology of human noroviruses and updates on vaccine development. Curr. Opin. Gastroenterol. 30, 25–33.

Scheres, S.H.W., 2012. RELION: implementation of a Bayesian approach to cryo-EM structure determination. J. Struct. Biol. 180, 519–530.

Singh, B.K., Leuthold, M.M., Hansman, G.S., 2015. Human noroviruses' fondness for histo-blood group antigens. J. Virol. 89, 2024–2040.

Tan, M., Jiang, X., 2005. The p domain of norovirus capsid protein forms a subviral particle that binds to histo-blood group antigen receptors. J. Virol. 79, 14017–14030.

Tan, M., Huang, P., Meller, J., Zhong, W., Farkas, T., Jiang, X., 2003. Mutations within the P2 domain of norovirus capsid affect binding to human histo-blood group antigens: evidence for a binding pocket. J. Virol. 77, 12562–12571.

Taniguchi, K., Urasawa, S., Urasawa, T., 1981. Further studies of 35-40 nm virus-like particles associated with outbreaks of acute gastroenteritis. J. Med. Microbiol. 14, 107–118.

Treanor, J.J., Atmar, R.L., Frey, S.E., Gormley, R., Chen, W.H., Ferreira, J., Goodwin, R., Borkowski, A., Clemens, R., Mendelman, P.M., 2014. A novel intramuscular bivalent norovirus virus-like particle vaccine candidate—reactogenicity, safety, and immunogenicity in a phase 1 trial in healthy adults. J. Infect. Dis. 210, 1763–1771.

Vinje, J., 2015. Advances in laboratory methods for detection and typing of norovirus. J. Clin. Microbiol. 53, 373–381.